

Mutations in *MYLPF* Cause a Novel Segmental Amyoplasia that Manifests as Distal Arthrogryposis

Jessica X. Chong,^{1,2,23} Jared C. Talbot,^{3,4,22,23,*} Emily M. Teets,³ Samantha Previs,⁵ Brit L. Martin,⁶ Kathryn M. Shively,¹ Colby T. Marvin,¹ Arthur S. Aylsworth,⁷ Reem Saadeh-Haddad,⁸ Ulrich A. Schatz,⁹ Francesca Inzana,¹⁰ Tawfeg Ben-Omran,¹¹ Fatima Almusafri,¹¹ Mariam Al-Mulla,¹¹ Kati J. Buckingham,¹ Tamar Harel,¹² Hagar Mor-Shaked,¹² Periyasamy Radhakrishnan,¹³ Katta M. Girisha,¹³ Shalini S. Nayak,¹³ Anju Shukla,¹³ Klaus Dieterich,^{14,15} Julien Faure,^{15,16} John Rendu,^{15,16} Yline Capri,¹⁷ Xenia Latypova,^{15,16} Deborah A. Nickerson,^{2,18} David M. Warshaw,⁵ Paul M.L. Janssen,⁶ University of Washington Center for Mendelian Genomics, Sharon L. Amacher,^{3,4,19,20} and Michael J. Bamshad^{1,2,18,21,*}

We identified ten persons in six consanguineous families with distal arthrogryposis (DA) who had congenital contractures, scoliosis, and short stature. Exome sequencing revealed that each affected person was homozygous for one of two different rare variants (c.470G>T [p.Cys157Phe] or c.469T>C [p.Cys157Arg]) affecting the same residue of *myosin light chain, phosphorylatable, fast skeletal muscle (MYLPF)*. In a seventh family, a c.487G>A (p.Gly163Ser) variant in *MYLPF* arose *de novo* in a father, who transmitted it to his son. In an eighth family comprised of seven individuals with dominantly inherited DA, a c.98C>T (p.Ala33Val) variant segregated in all four persons tested. Variants in *MYLPF* underlie both dominant and recessively inherited DA. Mylpf protein models suggest that the residues associated with dominant DA interact with myosin whereas the residues altered in families with recessive DA only indirectly impair this interaction. Pathological and histological exam of a foot amputated from an affected child revealed complete absence of skeletal muscle (i.e., segmental amyoplasia). To investigate the mechanism for this finding, we generated an animal model for partial MYLPF impairment by knocking out zebrafish *mylpfa*. The *mylpfa* mutant had reduced trunk contractile force and complete pectoral fin paralysis, demonstrating that *mylpf* impairment most severely affects limb movement. *mylpfa* mutant muscle weakness was most pronounced in an appendicular muscle and was explained by reduced myosin activity and fiber degeneration. Collectively, our findings demonstrate that partial loss of MYLPF function can lead to congenital contractures, likely as a result of degeneration of skeletal muscle in the distal limb.

Introduction

The distal arthrogryposes (DA) are a group of Mendelian conditions with overlapping phenotypic characteristics, shared genetic etiologies, and similar pathogenesis.¹ Clinically, the DAs are characterized by non-progressive congenital contractures of the limbs, most commonly affecting the hands, wrists, feet, and ankles. Congenital contractures of the face, ocular muscles, neck webbing, pterygia, short stature, and scoliosis are less frequent, variable findings that facilitate delineation among the most common DA conditions: DA1² (MIM: 108120), DA2A³ (Freeman-Sheldon syndrome [MIM: 193700]), and DA2B⁴

(Sheldon-Hall syndrome [MIM: 601680]). Variants in any one of sixteen different genes can underlie DA but the overwhelming majority of known pathogenic variants occur in just five genes: *TPM2* (MIM: 190990), *TNNI2* (MIM: 191043), *TNNT3* (MIM: 600692), *MYH3* (MIM: 160720), and *MYH8* (MIM: 160741).^{5,6} Nevertheless, collectively pathogenic variants are identified in only ~60% of families diagnosed with a DA, so the precise genetic etiology remains unknown in nearly half of DA-affected families.

Most of the genes that underlie DA encode sarcomeric components of skeletal muscle fibers. Thus, genes encoding sarcomeric proteins have long been considered

¹Division of Genetic Medicine, Department of Pediatrics, University of Washington, Seattle, WA 98195, USA; ²Brotman-Baty Institute, Seattle, WA 98195, USA; ³Department of Molecular Genetics, The Ohio State University, Columbus, OH 43210, USA; ⁴Center for Muscle Health and Neuromuscular Disorders, Columbus OH 43210, USA; ⁵Department of Molecular Physiology and Biophysics, University of Vermont, Burlington, VT 05405, USA; ⁶Department of Physiology and Cell Biology, The Ohio State University, Columbus, OH 43210, USA; ⁷Departments of Pediatrics and Genetics, University of North Carolina, Chapel Hill, NC 27599, USA; ⁸Division of Genetics, Department of Pediatrics, Medstar Georgetown University Hospital, Washington, DC 20007, USA; ⁹Human Genetics, Medical University, Innsbruck 6020, Austria; ¹⁰Genetic Counseling Service, Department of Pediatrics, Regional Hospital of Bolzano, Bolzano 39100, Italy; ¹¹Division of Genetic and Genomic Medicine, Sidra Medicine and Hamad Medical Corporation, PO Box 3050, Doha, Qatar; ¹²Department of Genetics, Hadassah-Hebrew University Medical Center, Jerusalem 91120, Israel; ¹³Department of Medical Genetics, Kasturba Medical College, Manipal, Manipal Academy of Higher Education, Manipal 576104, India; ¹⁴Department of Medical Genetics, CHU Grenoble Alpes, Génétique Médicale, Grenoble 38700, France; ¹⁵Université Grenoble Alpes, Inserm, U1216, Grenoble Institut des Neurosciences, Grenoble 38706, France; ¹⁶Biochimie Génétique et Moléculaire, CHU Grenoble Alpes, Grenoble 38700, France; ¹⁷Department of Genetics, APHP-Robert DEBRE University Hospital, UF Génétique clinique, Paris 75019, France; ¹⁸Department of Genome Sciences, University of Washington, Seattle, WA 98195, USA; ¹⁹Dept of Biological Chemistry and Pharmacology, The Ohio State University, Columbus, OH 43210, USA; ²⁰Center for RNA Biology, The Ohio State University, Columbus, OH 43210, USA; ²¹Seattle Children's Hospital, Seattle, WA 98105, USA

²²Present address: School of Biology and Ecology, University of Maine, Orono, ME 04469, USA

²³These authors contributed equally to this work

*Correspondence: jared.talbot@maine.edu (J.C.T.), mbamshad@uw.edu (M.J.B.)

<https://doi.org/10.1016/j.ajhg.2020.06.014>

© 2020 American Society of Human Genetics.



priority candidates for DA. Sarcomeres are the fundamental contractile structure of muscle, wherein myosin-rich thick filaments interact with actin-based thin filaments to generate contractile force. Each skeletal muscle myosin heavy chain protein (MyHC) has two distinct light chain proteins bound to the myosin lever arm: an essential light chain that is nearest to the myosin head and a regulatory light chain protein that can be phosphorylated and is located closer to the myosin tail region.⁷ Light chain proteins are needed to stabilize the myosin lever arm so that myosin can generate maximum force and velocity as revealed by *in vitro* studies of isolated myosin extracts deficient in light chain proteins.^{8,9}

To discover novel genes underlying DA, we performed exome sequencing (ES) on 172 families in which pathological variants in genes known to underlie DA1, DA2A, and DA2B had not been identified via Sanger sequencing. We identified putative pathogenic variants in 80 (47%) of these families including 44 families with mutations in 20 genes not known to underlie DA. Affected individuals from two families, including an affected child (family B) who had complete absence of skeletal muscle (i.e., segmental amyoplasia) in a foot (Figure 1), were each homozygous for the same variant (c.470G>T) in the gene, *MYLPF*, which encodes the fast-type skeletal muscle regulatory light chain. Data sharing via MatchMaker Exchange (MME) and directly with commercial diagnostic labs identified six additional families with similar phenotypic features and rare variants in *MYLPF*, including two families in which the condition was transmitted from parent to offspring (Table 2, families G and H). The mouse *Mylpf* knockout mutant is born without skeletal muscle and dies soon after birth because of respiratory failure,¹⁰ suggesting that human pathogenic *MYLPF* variants are likely to be hypomorphic alleles. To test this hypothesis, we knocked out the more prominent of the two zebrafish *mylpf* genes, *mylpfa*, and characterized development and function of *mylpfa* mutant skeletal muscle.

Zebrafish are a well-established model for investigating muscle structure, development, and disease mechanisms.^{11–14} Zebrafish rapidly generate functional myofibers that produce both spontaneous and evoked contractions at 1 day post-fertilization (dpf). By this stage, muscle fiber type is also readily apparent, with fast-twitch muscles identified by expression of *mylpfa* and other markers.^{15–18} Between 1 and 3 dpf, muscle precursors migrate away from their origin to produce new *mylpfa*-positive muscles, including fin muscles and the posterior hypaxial muscle.^{19–23} Herein, we show that partial loss of *Mylpf* function in zebrafish can recapitulate DA1, demonstrate that variants in *MYLPF* underlie DA1, and use a zebrafish model to provide explanations for the limb muscle loss observed in DA1 due to pathogenic variants in *MYLPF*.

Material and Methods

Discovery Cohort

From our cohort of 463 families (1,582 individuals) with multiple congenital contractures, we selected 172 families in which pathological variants had not been identified. All studies were approved by the institutional review boards of the University of Washington and Seattle Children's Hospital and informed consent was obtained from each participant or their parents.

Exome Sequencing and Variant Analysis

ES (families A and B) was performed by the University of Washington Center for Mendelian Genomics as described previously.²⁴ In brief, data were annotated with the Variant Effect Predictor v.89²⁵ and analyzed using GEMINI 0.20.2.²⁶ Variants unlikely to impact protein-coding sequence (for which GEMINI impact_severity = LOW), variants flagged by the Genome Analysis Toolkit (GATK) as low quality, and variants with an alternative allele frequency > 0.005 in any super-population in EVS/ESP6500, 1000 Genomes (phase 3 release), or the gnomAD Browser (v.2.0.1) were excluded. Variants that were frequent (alternative allele frequency > 0.5) in an internal database of >7,500 individuals (Geno2MP v.1.7 release) were excluded. Candidate genes were identified by filtering under these parameters for variants matching the predicted pattern of inheritance (i.e., autosomal *de novo*, homozygous recessive, compound heterozygous, X-linked *de novo*, X-linked recessive, and X-linked dominant models). Sequencing and analysis of all other families (C–H) were completed in a clinical/diagnostic setting. Average depth of coverage in family A was 46×, with 80% of the exome covered at >20×. Depth of coverage in all other families was at minimum ~80×. Segregation was performed by Sanger sequencing.

Fish Maintenance and Husbandry, Transgenes, and Mutant Construction

All animal protocols used in this study are approved by the Institutional Animal Care and Use Committees at The Ohio State University, the University of Vermont, and the University of Maine. Standard practices were used for zebrafish husbandry and maintenance.²⁷ Transgenic and mutant zebrafish strains were maintained on the AB wild-type background. Transgenic lines used in this study are *Tg(mylpfa:lyn-Cyan)fb122*,²⁸ *Tg(myog:Hsa.HIST1H2B-mRFP)fb121* (abbreviated *myog:H2B-mRFP*),²⁹ and *Tg(smyhc1:EGFP)i104*,³⁰ which are combined in a “3MuscleGlow” triple-transgenic line.³¹ The two *mylpfa* mutant lines described in this study were generated using established CRISPR-Cas9 protocols.³² One-cell embryos were injected with Cas9 mRNA and guide RNA targeting exon 2 (5'-TTGAGGCCAACACGTCCCTA-3') or exon 3 (5'-GGTGAAGTTGATTGGGCCGC-3'), raised to adulthood, and outcrossed. F1 progeny were screened using HRMA to identify founders carrying CRISPR-induced *mylpfa*^{oz43} and *mylpfa*^{oz30} lesions. All lesions were sequence confirmed in homozygotes. Mutations were outcrossed at least two generations after CRISPR injection before phenotypic analyses.

Zebrafish Immunohistochemistry and RNA *In Situ* Hybridization

Embryos and larvae carrying the *Tg(smyhc1:EGFP)i104* transgene were fixed and immunolabeled with Rbfox11 (1:500)³³ and F310 (1:100, Developmental Studies Hybridoma Bank) antibodies. RNA *in situ* hybridization was performed as described³⁴ using

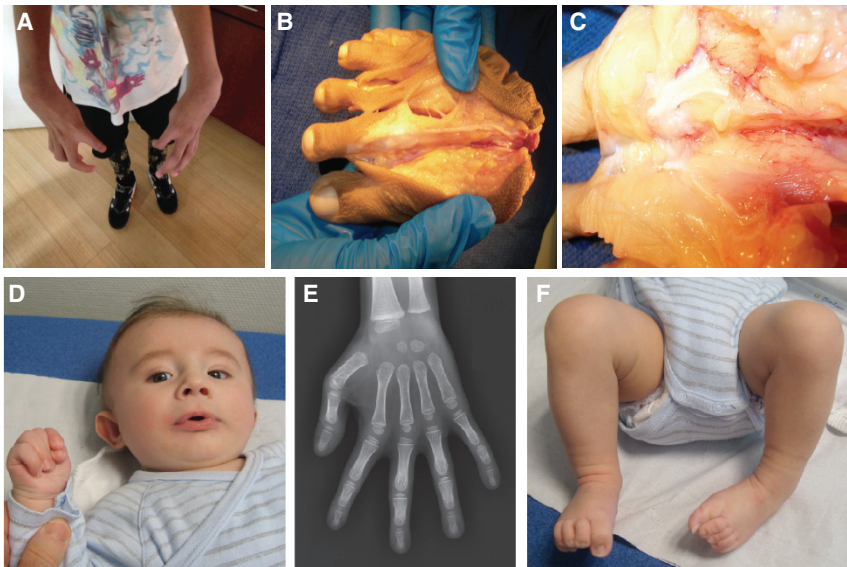


Figure 1. Phenotypic Characteristics of Individuals with Recessive or Dominant Distal Arthrogyposis Type 1 due to Variants in *MYLPF*

(A–C) Characteristics shown in family B II-1 with recessive DA1.

(A) Camptodactyly of the fingers and radial deviation of the wrists.

(B and C) Gross pathology of the right foot illustrating absence of skeletal muscles.

(D–F) Characteristics in family H IV-1 with dominant DA1: (D) pursed lips, camptodactyly of the fingers, adducted thumbs, (E) clinodactyly of the fifth digit, and (F) bilateral clubfoot. [Table 2](#) contains a detailed description of the phenotype of each affected individual and [Figure S1](#) provides a pedigree of each family with DA1 due to variants in *MYLPF*.

*mylpfa*¹⁸ and *mylpfb* riboprobes. For the latter, a 408 bp *mylpfb* fragment was amplified from zebrafish cDNA using forward 5'-AGTGGCCCCATCAACTTTACTG-3' and reverse 5'-AGCCCAAATGCCAACAAACC-3' primers and cloned into a PCR4-TOPO vector for subsequent probe synthesis.

Live Imaging of Muscle Structure

The following transgenes were used for live imaging: *Tg(mylpfa:lyn-Cyan)fb122*²⁸ to visualize fast muscle membranes, *Tg(myog:H2B-mRFP)*²⁹ to visualize myonuclei, and *Tg(smyhc1:EGFP)i104*³⁰ to visualize slow muscle fibers. Time-lapse imaging was performed as described.²³ For 3.25 dpf (78 hpf) and 4.25 dpf (102 hpf) comparisons, fish were dismantled and raised at 28.5°C between imaging sessions.

Muscle Contractile Force Measurement

Contractile analysis of 3 dpf larvae was performed as described previously.³⁵ Live 3 dpf larvae were anesthetized in 0.02% weight/volume tricaine buffered with Tris·HCl in Krebs-Henseleit solution and mounted on a custom-built set up between a force transducer and a hook. Larvae were stimulated at increasing frequencies and contractile strength measured. The maximal contractile force reached during each contraction was recorded, analyzed, and reported per larva. Fused tetanic contractions occur at 180 Hz. Measurements were compared at each contraction frequency using ANOVA followed by Tukey-Kramer post hoc comparisons.

Behavioral Analysis

To quantify fin movement, we recorded fish for one full minute, recorded the number of beats on each side of the fish, and then averaged fin movements per side. Escape response was evoked by gentle probing.³⁶ Freely moving fish were imaged using a Leica DMC5400 camera mounted on a Leica MZ10F microscope; images were collected in LAS X software and processed in FIJI.

Assessing Isolated Myosin Molecular Function

Zebrafish carrying *mylpfa*^{oz30} and *mylpfa*^{oz43} mutations were intercrossed, raised to 2 dpf, and sorted for wild-type or mutant swimming behavior. Proper sorting of mutant versus wild-type sibling

embryo genotypes was confirmed on more than 100 fish per group. At 4 dpf, fish were prepared, myosin extracted, and the *in vitro* motility assay was performed as described in the [Supplemental Material and Methods](#). Fish were dechorionated, de-yolked, permeabilized, and cut open through the abdomen to expose the de-membranated muscle fibers to subsequent solutions. Two fish larvae were inserted, tail first, into a flow cell constructed from a microscope slide and coverslip, as described previously.³⁷ Myosin Extraction Buffer was infused and incubated for 1 h, followed by 0.5 mg/mL BSA in Actin Buffer and incubated for 2 min at 30°C. All solution changes after this point were identical to that previously reported.³⁸ In brief, unlabeled actin was infused to effectively eliminate non-functional myosin heads, and then followed by rhodamine-phalloidin labeled actin in Motility Buffer containing ATP. Imaging and actin filament tracking and velocity analysis were conducted as previously described.³⁹ Each flow cell contained myosin from two fish, and at least four fields of view were imaged with at least 20 fluorescent actin filaments tracked per field. Velocity of these tracks was averaged across all fields of view for a single statistical N. Experiments for a given group were repeated on 4 flow cells minimum with at least two fully independent replicates on separate imaging days. For illustrative purposes in [Figure 3L](#) and [Video S3](#), actin filaments were tracked using the MTrackJ function in FIJI. Actin filament particles that stayed in the viewing frame throughout 100 frames of imaging were randomly selected and tracked for both wild-type sibling and *mylpfa*^{oz30} mutant genotypes.

Protein Analysis

Protein models were downloaded from PDB and visualized using Geneious software. Structures shown have the following PDB accession numbers: scallop, PDB: IKK7;⁴¹ squid, PDB: 315H;⁴² chicken, PDB: 2W4G;⁴³ rabbit, PDB: 5H53.⁴⁴ Protein alignments were produced by a MUSCLE algorithm in Geneious software. Protein sequences with the following accession numbers were downloaded from NCBI, Ensembl, or Uniprot: human *MYLPF* (GenBank: NP_037424.2), *Mus musculus* (mouse) *Mylpf* (GenBank: NP_058034.1), *Oryctolagus cuniculus* (rabbit) *Mylpf* (GenBank: NP_001076230.2), *Gallus gallus* (chicken) *Mylpf* (GenBank: NP_001185673.1), *Xenopus tropicalis* (frog) *Mylpf* (Uniprot:

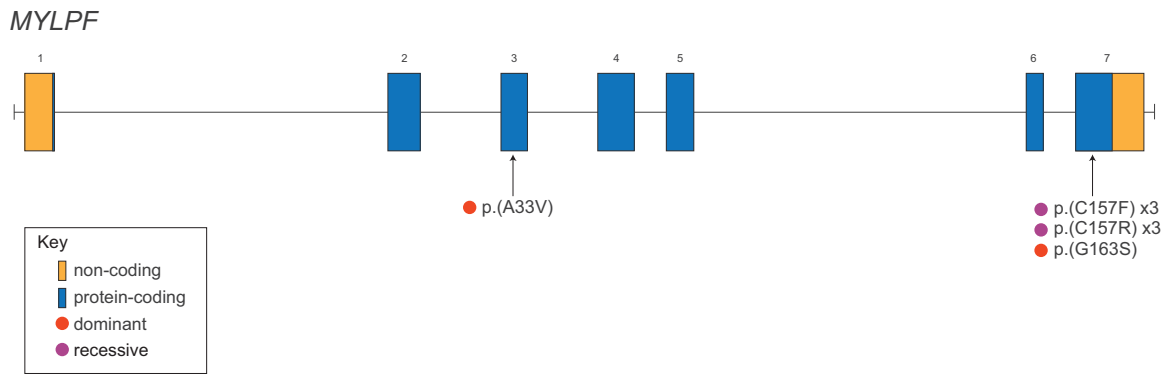


Figure 2. Genomic Model of MYLPP

MYLPP is composed of seven exons, each of which consists of protein-coding (blue) and non-coding (orange) sequence. The approximate location of each pathogenic variant is indicated by an arrow. The p.Cys157Phe (p.C157F) and p.Cys157Arg (p.C157R) variants are each found in three families (×3) and lead to a recessive phenotype (purple circle). The p.Ala33Val (p.A33V) and p.Gly163Ser (p.G163S) variants lead to a dominant phenotype (red circle).

CAJ83266.1), *Danio rerio* (zebrafish) Mylpfa (GenBank: NP_571263.1), *Danio rerio* (zebrafish) Mylpfb (GenBank: NP_001004668.1), *Callorhynchus milii* (elephant shark) skeletal Myl2 (AFP05921.1), *Eptatretus burgeri* (hagfish) Myl2 (Ensembl: ENSEMBUT00000005213.1), *Todarodes pacificus* (Japanese flying squid) light chain-2 (LC2; Uniprot: P08052), *Chlamys nipponensis akazara* (Japanese bay scallop) myosin light chain regulatory (MLR; Uniprot: P05963), *Dictyostelium discoideum* (Dicty) RLC (Uniprot: AAA33226.1), and *Saccharomyces cerevisiae* (yeast) Mlc2 (ONH78313.1). The human MYLPP orthologs shown are regulatory light chain genes MLC2 (GenBank: NP_000423.2), MLC5 isoform 1 (GenBank: NP_002468.1), MLC7 (Uniprot: AAH27915.1), MLC9 isoform A (GenBank: NP_006088.2), MLC10 (Ensembl: ENST00000223167.4), MLC12A (GenBank: NP_001289977.1), and MLC12B (GenBank: NP_001138417.1) as well as essential light chains MLC1 (GenBank: NP_524144), MLC3 (GenBank: NP_524146.1), MLC4 (GenBank: NP_001002841.1), MLC6 isoform 1 (GenBank: NP_066299.2), and MLC6 isoform 2 (GenBank: NP_524147.2). Expression patterns are described previously.^{45–47}

Results

Identification of Variants in MYLPP

Family A, of European ancestry, consisted of two affected siblings born to unaffected parents. Analysis of high-density genotyping data suggested that their parents were consanguineous ($F = 0.0189$). This observation was later confirmed by review of pedigree records that documented the parents were second cousins once removed. Each affected child, a male last evaluated at 13 years of age and a female last examined at 24 years of age, had severe contractures of the hands, fingers, wrists, elbows, hips, knees, ankles, and neck; pterygia of the elbows and knees; small mouths; and short stature (<1 percentile for weight and at ~1.1 percentile for height) (Table 1). Family B comprised an adopted child of East Indian ancestry whose parents were predicted to be first cousins based on analysis of high-density genotyping data ($F = 0.0657$) and who was homozygous for the same variant as found in the siblings in family A. The proband of family B, last examined at 6

years of age, also had similar clinical findings to the siblings in family A including a small mouth, micrognathia, scoliosis, contractures of the hands and wrists, and severe right clubfoot that was recalcitrant to treatment, ultimately leading to amputation of the lower leg. Pathological exam of the foot revealed complete absence of skeletal muscle that was confirmed histologically (Figure 1). In both families, we identified homozygosity for a variant (c.470G>T, rs756765686) in a single gene, *myosin light chain, phosphorylatable fast skeletal muscle* (MYLPP [MIM: 617378; Refseq: NM_013292.4]) (Table 1; Figure 2). This variant is predicted to result in p.Cys157Phe substitution and has a CADD (v.1.6) score of 27.5. MYLPP had been considered *a priori* to be a high-priority DA candidate gene because of its role in development of skeletal muscle.¹⁰ Sanger sequencing validated homozygosity of the c.470G>T variant in all affected persons and that the parents in family A were heterozygous carriers. These results suggested that homozygosity for c.470G>T in MYLPP resulted in a pattern of multiple congenital contractures virtually indistinguishable from that observed in persons with DA, specifically DA1.

In an effort to find additional families with a pathogenic variant in MYLPP and clinical characteristics of DA1, we submitted genetic data and phenotypic information to the MatchMaker Exchange (MME) via the MyGene2 node and identified two additional families (E and F) that had been submitted to the GeneMatcher node. Simultaneously, we queried commercial genetic testing companies and colleagues about families in which MYLPP had been identified as a candidate gene. One commercial lab, GeneDx, responded that clinicians for two families (C and D) had agreed to be contacted by us and provide de-identified genetic and phenotypic information for review.

The proband of family C was a female, born in Pakistan to unaffected parents, and last evaluated at 29 years of age. She had short stature, nearsightedness, mild conductive hearing loss diagnosed in adulthood, scoliosis, bilateral clubfeet, and multiple congenital

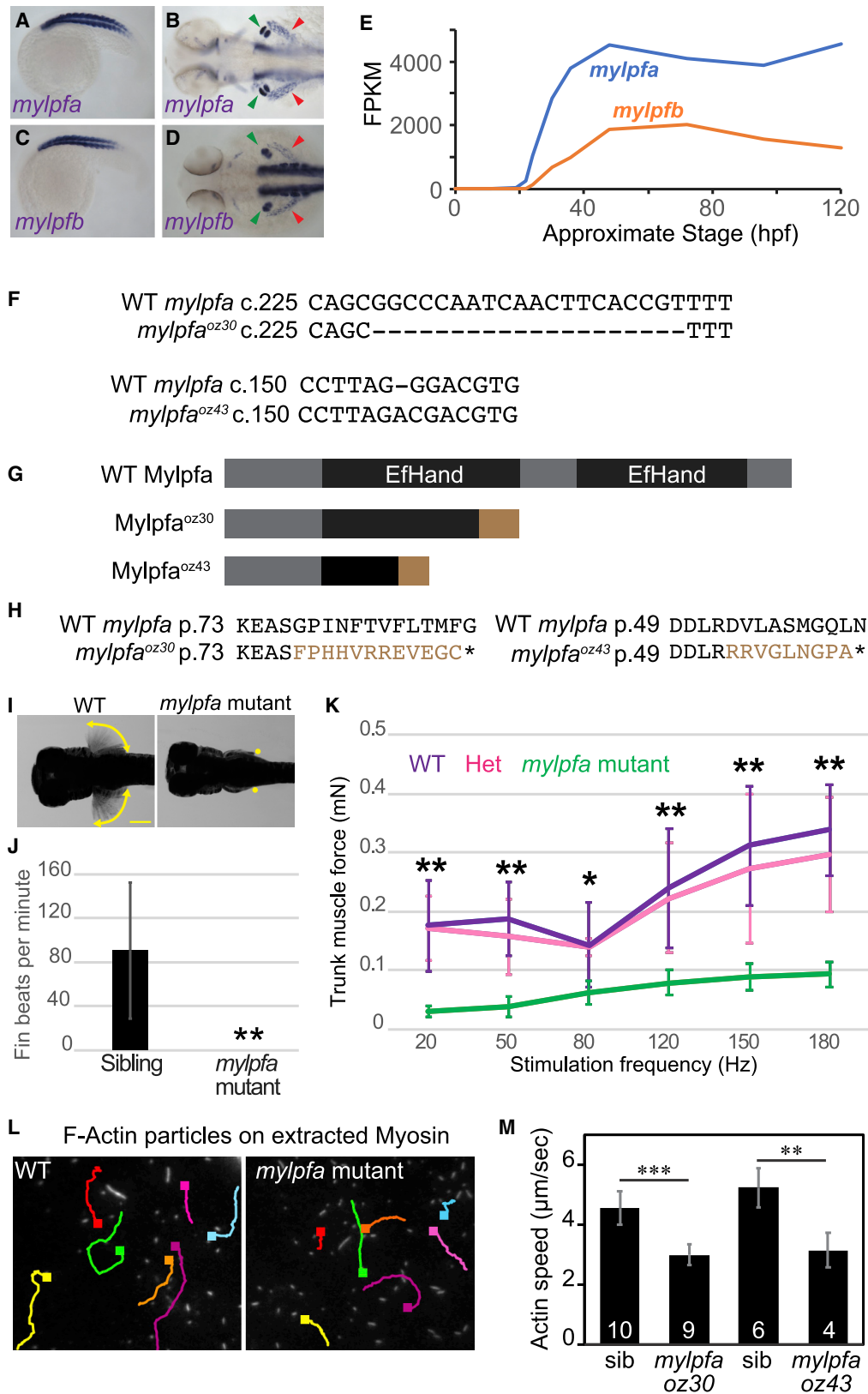


Figure 3. Zebrafish *mylpfa* Mutants Have Weakened Myotomes and Paralyzed Fin Muscle

(A–D) RNA *in situ* hybridization showing (A, B) *mylpfa* and (C, D) *mylpfb* expression at 20 hpf (A, C) and 52 hpf (B, D). Both genes are expressed exclusively in fast muscle, including somitic muscles, fin muscle (green arrowhead), and posterior hypaxial muscle (red arrowhead).

(E) Transcript abundance of *mylpfa* (blue) and *mylpfb* (orange) through early larval development, using data provided in the EMBL-EBI expression atlas.⁴⁰

(legend continued on next page)

contractures including the hands, wrists, elbows, and shoulders. ES demonstrated that she was homozygous for the variant, c.469T>C (p.Cys157Arg) (rs748809300) in *MYLPF*, with a CADD score of 25.2. Family D consisted of an affected stillborn female born to unaffected, first cousin parents from Pakistan. At 35 weeks estimated gestational age, a prenatal ultrasound demonstrated polyhydramnios, shortened long bones, “clenched hands,” and bilateral clubfeet. The fetus was subsequently stillborn and postmortem examination confirmed the prenatal findings. Proband-only ES of the fetus demonstrated she was also homozygous for c.469T>C in *MYLPF*. The proband of family E was a male of Pakistani ancestry, whose parents were first cousins. At ~13 weeks gestational age, a prenatal ultrasound detected nuchal edema, a septated cystic hygroma, mild enlarged renal pelvis, and normal amniotic fluid. At 19 weeks gestational age, an ultrasound showed decreased fetal movements with fetal hypokinesia and akinesia of lower limbs, clubfeet, thoracic kyphosis and scoliosis, generalized edema (trunk and nuchal), and normal amniotic fluid volume. He had multiple congenital contractures of the hands, wrists, elbows, shoulders, hips, knees, and bilateral clubfeet as well as pterygia of the neck. He died at 1 month of age and was found to be homozygous for the c.469T>C variant in *MYLPF* found in families C and D. Both parents were heterozygous.

Family F (Table 1 and Figure S1) is a large kindred from South India in which four individuals were each homozygous for c.470G>T in *MYLPF*. Individuals III-2 and III-3 were the offspring of a consanguineous marriage between II-1 and II-2 whereas individuals III-5 and III-6, who had two affected fetuses (IV-8 and IV-10), were not known to be closely related but grew up in the same community. Individual III-3 and both affected fetuses (IV-8 and IV-10) had contractures of the hands and feet, while III-2 had contractures of only the hands. None of the heterozygous car-

riers tested (II-1, II-2, III-5, and III-6) had congenital contractures.

Collectively, we identified two unique missense variants affecting the same residue, p.Cys157, in *MYLPF* in ten individuals in six unrelated families (A–F) who had been diagnosed with multiple congenital contractures. Both missense variants are exceedingly rare (maximum frequency in any super-population in gnomAD = 0.00013 in South Asians for c.470G>T and 0.00009 in Finnish for c.469T>C, and no homozygotes reported) among >151,000 individuals included in publicly available databases: 1000 Genomes phase 3, the gnomAD browser (v.2.0.2), or UK10K (February 15, 2016 release) and have high Phred-scaled CADD scores, consistent with pathogenic dominant variants (Table 1). High-density chip genotype data (Illumina Human Core Exome) was available for one affected individual of East Indian ancestry (family B) and one affected individual in the family of Polish ancestry (family A), both of whom were homozygous for the first variant, c.470G>T. We searched for a shared haplotype that would provide evidence that this variant is a founder mutation, but their genotypes differed at even the nearest SNP flanking the variant (both C/C at chr16:30368510 [rs13335932]; both homozygous for c.470G>T at chr16:30389181; but at chr16:30393147 [rs34518080], the Polish individual was A/A while the East Indian individual was C/C), leaving at most a short shared haplotype. Combined with the observation of this variant in multiple populations in gnomAD, it seems likely that this variant has either arisen independently in different populations or early in human history. In contrast, the variant shared among all three Pakistani families, c.469T>C, may be a founder mutation based on their shared ancestry, but we were unable to obtain the original exome sequence data to confirm the presence of a shared haplotype.

In a seventh family (family G, Table 2), a 1-year-old male proband was found to be heterozygous for a c.487G>A

(F) Alignment of wild-type (WT) and mutant genomic sequence across the *mylpfa*^{oz30} and *mylpfa*^{oz43} lesions. *mylpfa*^{oz30} is a 20 bp deletion within exon 3 predicted to frameshift the 169 amino acid protein after amino acid 76, and *mylpfa*^{oz43} is a 1 bp deletion within exon 2 predicted to frameshift the protein after amino acid 52.

(G) Diagram of wild-type and predicted mutant Mylpfa proteins. Both mutant alleles should truncate the protein within the first EF-hand domain (black boxes) and introduce short stretches of aberrant amino acids after the frameshift (brown).

(H) Alignment of wild-type and predicted mutant proteins in the region of frameshift, showing normal sequence (black) and aberrant residues (brown).

(I) Superimposed time-lapse images (from Video S1) showing fin motion in a wild-type embryo (yellow crescent arrows) and motionless fins in a *mylpfa*^{oz30} mutant (yellow dots) at 4 dpf. Similar results were obtained using a second mutant allele, *mylpfa*^{oz43} (not shown).

(J) Quantification of fin beats per minute averaged over left and right sides, in *mylpfa*^{oz30} mutant (n = 12) or phenotypically wild-type sibling (n = 12) fish at 4 dpf. We have never observed a fin beat in more than 100 *mylpfa*^{oz30} and *mylpfa*^{oz43} mutant fish examined.

(K) Trunk muscle contractile force in *mylpfa*^{oz30} and wild-type or heterozygous siblings at 3 dpf. No significant differences are found between wild-type and heterozygous fish. However, homozygous *mylpfa* mutant fish are significantly weaker than non-mutant siblings at all stimulation frequencies.

(L) Representative image of fluorescently labeled actin filaments tracked in the *in vitro* motility assay, with colored lines showing traces of individual filaments over 50 frames of imaging (2.5 s). Within this time period, actin filaments on wild-type myosin extracts typically move further than do filaments on *mylpfa* mutant myosin extracts.

(M) Actin filament speeds measured using the *in vitro* motility assay generated by extracted myosin. Myosin from *mylpfa* homozygous mutant fish propel actin filaments significantly slower than myosin from wild-type siblings. Numbers shown in each bar indicate the experimental N; each experiment uses myosin extracted from two fish (see Material and Methods). Asterisks in (J, K, M) indicate p thresholds for the WT/het pools versus mutant; *p < 0.05, **p < 0.001, ***p < 0.0001. Error bars in (J, K, M) represent standard deviation. Statistical comparisons in (J) and (M) use Student's t test; in (K), thresholds are determined by ANOVA followed by Tukey-Kramer comparisons. Scale bar in (I) is 250 μm.

Table 1. Families A–F: Mutations and Clinical Findings of Individuals with Recessive Distal Arthrogyrosis Type 1 due to Variants in MYLPP

Family	A	A	B	C	D	E	F	F	F	F
Ancestry	Polish	Polish	Indian	Pakistani	Pakistani	Pakistani	Indian	Indian	Indian	Indian
Individual	VI-1	VI-2	II-1	II-1	IV-2	II-1	IV-8	IV-10	III-2	III-3
Sex	male	female	male	female	female	male	unknown	female	female	female
Age at last assessment	13 years	24 years	6.5 years	29 years	35 weeks	at birth (37+2 gestational weeks)	12 weeks gestation (antenatal ultrasound)	19 weeks gestation (perinatal autopsy)	38 years	36 years
Variant										
cDNA change	c.470G>T	c.470G>T	c.470G>T	c.469T>C	c.469T>C	c.469T>C	c.470G>T	c.470G>T	c.470G>T	c.470G>T
Genomic coordinates	chr16:g.30389181G>T	chr16:g.30389181G>T	chr16:g.30389181G>T	chr16:g.30389180T>C	chr16:g.30389180T>C	chr16:g.30389180T>C	chr16:g.30389181G>T	chr16:g.30389181G>T	chr16:g.30389181G>T	chr16:g.30389181G>T
CADD score	27.5	27.5	27.5	25.2	25.2	25.2	27.5	27.5	27.5	27.5
Amino acid change	p.Cys157Phe	p.Cys157Phe	p.Cys157Phe	p.Cys157Arg	p.Cys157Arg	p.Cys157Arg	p.Cys157Phe	p.Cys157Phe	p.Cys157Phe	p.Cys157Phe
Genotype	homozygous	homozygous	homozygous	homozygous	homozygous	homozygous	homozygous	homozygous	homozygous	homozygous
Inheritance	recessive	recessive	recessive	recessive	recessive	recessive	recessive	recessive	recessive	recessive
Growth										
Weight %ile	<1	8	8.8	<1	ND	3–10 (1,820 g)	ND	50 (249 g)	ND	ND
Height %ile	1.1	ND	<1	<1	ND	ND	ND	48 (22 cm)	ND	ND
Head and Neck										
Small mouth (HP:0000160)	+	+	+	–	ND	–	–	+, retrognathia (HP:0000278)	–	–
Lip/palate	cleft lip & palate (HP:0410030, HP:0000175)	cleft lip & palate (HP:0410030, HP:0000175)	–	–	ND	–	ND	thin vermilion (HP:0000233), bifid uvula (HP:0000193)	–	thin vermilion (HP:0000233)
Limited neck rotation (HP:0005986)	+	+	+	+	ND	–	–	–	–	–
Skeletal										
Scoliosis (HP:0002650)	+	+	+	+	ND	+	–	–	–	–
Short stature (HP:0004322)	+	+	+	+	+	ND	ND	–	ND	ND

(Continued on next page)

Table 1. Continued

Family	A	A	B	C	D	E	F	F	F	F
Hip contractures (HP:0003273)	+	+	ND	+	ND	+	ND	+	–	–
Elbow contractures (HP:0002987)	+	+	–	+	ND	+	ND	–	–	–
Knee contractures (HP:0006380)	+	+	–	+	–	+	ND	+	–	–
Camptodactyly, fingers (HP:0100490)	+	+	+	+	–	+	ND	+	+	+
Vertical talus (HP:0001838)	+	+	–	–	–	–	ND	–	ND	ND
Equinovarus (HP:0001762)	–	–	+	+	+	+	+	+	–	+
Camptodactyly, toes (HP:0001836)	–	–	+	–	–	–	ND	–	ND	ND
Contractures of wrists (HP:0001239)	–	–	+	+	–	+	ND	ND	+	+
Other										
Undescended testicles (HP:0000028)	+	NA	+	NA	NA	–	ND	–	NA	NA
Other	none	none	none	none	none	short neck (HP:0000470)	increased nuchal translucency	short neck (HP:0000470)	none	none

Summary of clinical features of affected individuals from families A–F in which mutations in *MYLPF* were identified. Clinical characteristics listed in the table are primarily features that delineate DA1. Plus (+) indicates presence of a finding, minus (–) indicates absence of a finding. ND, no data were available; NA, not applicable; CADD, Combined Annotation Dependent Depletion v.1.6. cDNA positions named using HGVS notation and RefSeq transcript NM_013292.5. Predicted amino acid changes are shown. c.470G>T (p.Cys157Phe) has been reported in dbSNP as rs756765686 and in ClinVar under accession VCV000916685. c.469T>C (p.Cys157Arg) is in dbSNP as rs748809300 and ClinVar as VCV000916686. c.98C>T (p.Ala33Val) is in ClinVar as VCV000916688 and c.487G>A (p.Gly163Ser) as VCV000916687.

Table 2. Families G and H: Mutations and Clinical Findings of Individuals with Dominant Distal Arthrogryposis Type 1 due to Variants in MYLPF

Family	G	G	H	H	H	H	H
Ancestry	Ashkenazi Jewish	Ashkenazi Jewish	French	French	French	French	French
Individual	II-1	III-1	IV-3	III-6	II-7	III-2	IV-1
Sex	male	male	female	female	female	female	male
Age at last assessment	>18 years	1 year	6 years	39 years	69 years	26 years	6 months
Variant							
cDNA change	c.487G>A	c.487G>A	c.98C>T	c.98C>T	c.98C>T	c.98C>T	c.98C>T
Genomic coordinates	chr16:g.30389198G>A	chr16:g.30389198G>A	chr16:g.30387467C>T	chr16:g.30387467C>T	chr16:g.30387467C>T	chr16:g.30387467C>T	chr16:g.30387467C>T
CADD score	32.0	32.0	31.0	31.0	31.0	31.0	31.0
Amino acid change	p.Gly163Ser	p.Gly163Ser	p.Ala33Val	p.Ala33Val	p.Ala33Val	p.Ala33Val	p.Ala33Val
Genotype	heterozygous	heterozygous	heterozygous	heterozygous	heterozygous	heterozygous	heterozygous
Inheritance	<i>de novo</i>	dominant	dominant	dominant	dominant	dominant	dominant
Growth							
Weight %ile	ND	<3rd	+1.5 SD	−0.5 SD	+0.5 SD	ND	−1 SD
Height %ile	ND	ND	+0.5 SD	−0.5 SD	0 SD	ND	0 SD
Head and Neck							
Small mouth (HP:0000160)	ND	+, limited opening (HP:0000211)	+, retrognathia (HP:0000278)	+	+	+	+
Lip/palate	ND	high arched palate (HP:0000218)	−	−	−	pursed lips (HP:0000205)	pursed lips (HP:0000205), high arched palate (HP:0000218)
Limited neck rotation (HP:0005986)	ND	−	−	−	−	−	−
Skeletal							
Scoliosis (HP:0002650)	ND	−	−	−	−	+	−
Short stature (HP:0004322)	ND	ND	−	−	−	−	−
Hip contractures (HP:0003273)	ND	+	−	−	−	−	−

(Continued on next page)

Table 2. Continued

Family	G	G	H	H	H	H	H
Elbow contractures (HP:0002987)	ND	–	–	–	–	–	–
Knee contractures (HP:0006380)	ND	+	–	–	–	–	–
Camptodactyly, fingers (HP:0100490)	+	+	+	+	+	+	+
Vertical talus (HP:0001838)	ND	+	+ (right)	+	–	–	–
Equinovarus (HP:0001762)	ND	–	+ (left)	–	–	–	+
Camptodactyly, toes (HP:0001836)	ND	+	–	–	–	–	–
Contractures of wrists (HP:0001239)	+	–	+	+	+	+	+
Other							
Undescended testicles (HP:0000028)	ND	+	NA	NA	NA	NA	ND
Other	none	none	chin skin folds	shoulder contractures (HP:0003044)	shoulder contractures (HP:0003044)	adducted thumbs (HP:0001181), flexed metacarpophalangeal joints (HP:0006070), blepharophimosis (HP:0000581)	adducted thumbs (HP:0001181), flexed metacarpophalangeal joints (HP:0006070), fifth finger clinodactyly (HP:0004209)

Summary of clinical features of affected individuals from families G and H in which mutations in *MYLPF* were identified. See [Table 1](#) legend for details.

(p.Gly163Ser) variant that arose *de novo* in his father. The family was of Ashkenazi Jewish origin. The proband, last evaluated at 12 months of age, had multiple congenital contractures including bilateral camptodactyly and overriding fingers, adducted thumbs, ulnar deviation of the wrists, bilateral hip dislocations, and bilateral vertical talus. He had a mild kyphosis, bilateral inguinal hernias, small palpebral fissures, epicanthal folds, anteverted nares with hypoplastic alae nasae, long philtral folds, a thin upper lip, small mouth, high-arched palate without cleft, and micro-retrognathia. Because of recurrent apnea, he underwent a tracheostomy. His father had similar facial features, ulnar deviation of the hands, and had undergone multiple corrective procedures for contractures of the ankles. Manual review in IGV of the proband's exome sequence data did not reveal any additional rare variants in *MYLPPF* and no candidate variants were found in other genes known to underlie DA. Depth of sequencing of all exons of these genes was >10× and there was no evidence of a copy number variant that would explain his features. This variant had a CADD score of 32.0.

Family H is a family in which the two probands, individuals IV-1 and IV-3, were independently diagnosed with distal arthrogryposis (DA). Individual IV-3 was first evaluated at 7 months of age because of a bilateral ulnar finger deviation, flexed thumbs, right calcaneovalgus deformity, and left clubfoot. Several months later, her cousin (IV-1) was referred to an arthrogryposis clinic for evaluation of bilateral ulnar deviation and bilateral clubfoot (Figure 1). The mother and grandmother of each proband also had congenital contractures (Table 2). Individual IV-3, last evaluated at 6 years of age, has no growth retardation or scoliosis, and neither did her mother nor grandmother. Clinical exome sequencing of IV-3 and III-2 revealed heterozygosity for a c.98C>T (p.Ala33Val) (GenBank: NM_013292) and Sanger sequencing confirmed it was present in III-6 and II-7 (Table 2 and Figure S1). This variant is predicted to be damaging with a CADD score of 31.0 and is absent from gnomAD v.2.1.1 (accessed on 04/12/2020). Dominant inheritance of DA in families G and H suggest that p.Gly163Ser and p.Ala33Val may impact *MYLPPF* function more severely than the recessive variants, p.Cys157Phe and p.Cys157Ser.

Loss of Zebrafish *mylpf* Function Causes Muscle Weakness and Loss

Mylpf structure is highly conserved among vertebrates suggesting that function is also conserved. Previous studies showed that mice homozygous for a null *mylpf* allele lack all skeletal muscle at birth.¹⁰ However, these studies did not determine whether muscle failed to develop or underwent degeneration after normal development, nor did they explain how complete or partial loss of *MYLPPF* function in humans selectively and/or disproportionately affects muscles of the limb. To generate a vertebrate model for partial loss of function, we knocked out zebrafish *mylpfa*, one of the two zebrafish *Mylpf* orthologs. Both orthologs, *mylpfa* and *mylpfb*, are expressed specifically in embryonic and

larval fast-twitch myofibers,⁴⁸ with *mylpfa* being the predominantly expressed gene (Figures 3A–3E). These two genes encode proteins with more than 90% amino acid identity, differing at only 11 of 170 residues. We used CRISPR-Cas9-mediated mutagenesis to generate two independent *mylpfa* alleles, *mylpfa*^{oz30} and *mylpfa*^{oz43} (Figure 3F). Both alleles frameshift the protein within the first of two EF-hand domains (Figures 3G and 3H) and are thus predicted to be nulls. However, homozygous *mylpfa* mutant embryos are expected to retain some *Mylpf* function because they still have a functional *mylpfb* gene.

Pectoral fins of the *mylpfa* mutant are completely paralyzed, and the mutant has an impaired escape response (Figures 3I and 3J, Videos S1 and S2). To directly measure contractile strength of trunk muscle, we electrically stimulated live intact 3 dpf embryos mounted between a hook at the head and a force transducer at the tail. At all frequencies tested, *mylpfa*^{oz30} homozygous mutant embryos are significantly weaker than their unaffected siblings ($p < 0.001$ at 20 Hz and 180 Hz) (Figure 3K). To characterize the motion-generating capacity of myosin with their constituent light chains, we extracted monomeric myosin from *mylpfa* mutant and sibling wild-type fish onto the surface of a microscope flow cell chamber (see [Material and Methods](#)). Fluorescent, filamentous actin was introduced into the chamber and actin motion generated by the extracted myosin was imaged. We observed that the actin filament velocity was significantly slower in both *mylpfa*^{oz30} and *mylpfa*^{oz43} compared to wild-type siblings (Figures 3L and 3M, Video S3). The remaining and apparently compromised myosin motile function and contractile force observed could be due to residual *mylpf* function in fast-twitch muscles (provided by *mylpfb*) and/or intact slow-twitch muscles, which do not express *mylpfa* and appear normal (Figures 3A–3D and 4C–4F). Thus, like persons with DA, zebrafish *mylpfa* mutants display abnormal movement that is more pronounced in limbs; this weakness can be explained at least in part by impaired myosin force and motion generation in fast-twitch muscle.

We next examined zebrafish muscle over time, to learn whether *mylpfa* mutant muscles form and then deteriorate or whether they fail to develop in the first place. This distinction may be particularly important for understanding the complete absence of skeletal muscle that was observed in the foot of one child with DA associated with a p.Cys157Phe variant. Shortly after somite formation, *mylpfa* mutant muscle morphology appears normal (Figures 4A and 4B). However, at 6 days post-fertilization (dpf), *mylpfa* mutant myotomes are significantly ($p < 0.05$) reduced in dorsal-ventral height compared to wild-type (WT = 266 μm , $n = 12$; *mylpfa*^{-/-} = 232 μm , $n = 6$) and muscle fibers are irregularly shaped, suggesting that fast-twitch fibers deteriorate over time (Figures 4C and 4D). Slow-twitch muscle fibers are spared in the same fish (Figures 4E and 4F). Muscle defects are most pronounced in a specific appendicular muscle, the posterior hypaxial muscle (PHM) (Figures 4G–4J). Although the PHM forms

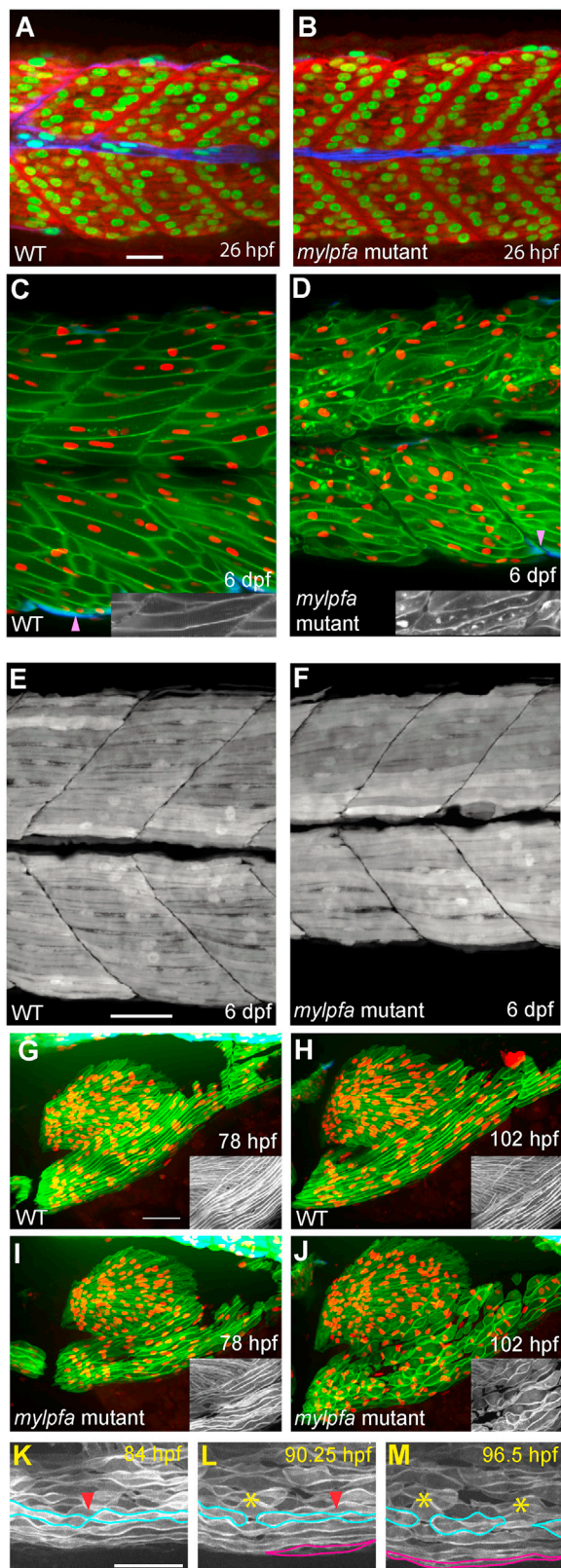


Figure 4. Embryonic Muscle Degenerates in *mylpfa* Mutant Zebrafish

(A and B) Confocal images showing muscle morphology at 26 hpf in wild-type (A) or *mylpfa*^{-/-} (B) embryos. Myonuclei are labeled using Rbfox11 immunolabeling (green), fast-twitch fibers are labeled using F310 immunolabeling (red),

at the normal time in *mylpfa* mutants and is initially comprised of multinucleate muscle, the muscle fibers break down into small “islands” that are often mononucleate by 4 dpf (Figures 4I and 4J). Muscle deterioration in the PHM is especially rapid compared to axial muscle, since axial muscle fibers form prior to appendicular fibers, yet are still relatively intact and multinucleate at 6 dpf (compare Figures 4D and 4J insets).

To examine whether *mylpfa* mutant PHM cellular islands are degenerated fibers or newly forming mononucleate myoblasts, we conducted confocal time-lapse microscopy beginning at 84 hpf (Figures 4K–4M; Video S4). At time-lapse outset, most PHM fibers are intact, with wavy membranes that occasionally are narrowed almost to closure (Figures 4K and 4L). Membrane irregularities become more pronounced over time, and pieces of fiber pinch off (Figures 4L and 4M). During each time-lapse (n = 3), a new PHM fiber was added (Figures 4L and 4M), suggesting that hyperplastic growth continued during the imaging period. Together, these findings indicate that zebrafish *mylpfa* is required to maintain myofiber integrity but is not required for initial myofiber formation or hyperplastic growth. Accordingly, we hypothesize that the segmental amyoplasia in individuals with pathogenic variants results from myofibers that form normally but subsequently degenerate.

Protein Modeling of MYLPF Variants

To better understand how MYLPF p.Cys157Phe and p.Cys157Arg variants versus the p.Ala33Val and p.Gly163Ser variants underlie recessive versus dominantly inherited DA, respectively, we examined a previously developed

and slow-twitch fibers are labeled using *Tg(smyhc1:EGFP)i104* (blue).

(C and D) Confocal z sections showing muscle morphology of live 6 dpf larvae expressing a fast muscle cell membrane transgene *Tg(mylpfa:lyn-Cyan)fb122* (green) and a myonuclear transgene *myog:H2B-mRFP* (red). These fish also express a slow muscle marker *Tg(smyhc1:EGFP)i104* (blue), which is largely lateral to the plane of focus; pink arrowheads point to slow muscle cells within the shown plane. Compared to wild-type controls (C), *mylpfa*^{-/-} myofibers have irregular membrane structure (D).

(E and F) Confocal projections of the same myotomes from (C) and (D) showing slow muscle fibers (white).

(G–J) Confocal projections of pectoral fin and PHM muscles, imaged on 3.25 dpf and again on 4.25 dpf, in fish expressing transgenes *Tg(mylpfa:lyn-Cyan)fb122* in fast muscle (green), *myog:H2B-mRFP* in all myonuclei (red), and *Tg(smyhc1:EGFP)i104* in slow muscle (blue). Fin muscle and PHM express *Tg(mylpfa:lyn-Cyan)fb122* but not *Tg(smyhc1:EGFP)i104*, as expected for muscles predominantly comprised of fast-twitch fibers.^{23,49} In striking contrast to wild-type (G, H), *mylpfa* mutant muscle fibers degenerate between 3.25 and 4.25 dpf (I, J).

(K–M) Images from a time-lapse of *mylpfa* mutant PHM degeneration (Video S3). Muscle fibers which initially appear wavy (aqua outline), often become narrow (red arrowheads) before breaking apart (asterisk). A myofiber that appears during imaging is outlined in magenta.

Insets in (C), (D), and (G)–(J) show *Tg(mylpfa:lyn-Cyan)fb122* in greyscale. Scale bars in (A) for (A) and (B), in (E) for (C)–(F), in (G) for (G)–(J), and in (K) for (K)–(M) are 50 μm.

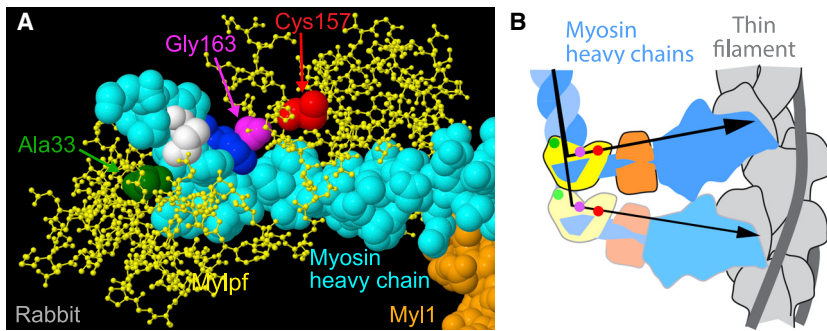


Figure 5. Mylpf Protein Sequence and Structure Comparisons Identify Key Conserved Residues

(A) Model of rabbit Mylpf protein in complex with the neck and head region of myosin heavy chain in rigor. The heavy chain (cyan) and essential light chain (orange) are rendered using a space-filling model and the light chain is shown using a ball and stick model (yellow) except for three residues that align with MYLPPF Ala33, Cys157, and Gly163, which are rendered in space filling models; we refer to these by their human numbering. Ala33 (green) is adjacent to a Lys residue in the heavy chain (white). Gly163 (magenta) directly contacts a Phe residue in the heavy chain (dark blue). In contrast, Cys157 (red) is found internal to Mylpf protein.

(B) Overview of myosin interaction with thin filaments, color-coded as in (A). Mylpf protein binds to the heavy chain region that bends toward the thin filament (arrows).

(C) Alignment of select vertebrate Mylpf proteins and invertebrate Mlc2 proteins highlighting conservation of Ala33, Cys157, and Gly163. The percent identity (% ident.) between human MYLPPF and aligned proteins is shown to the right of the alignments.

(D–G) Magnified views of myosin heavy and light chain genes showing how Ala33 and Gly163 positions vary between scallop⁴¹ (D), squid⁴² (E), chicken⁴³ (F), and rabbit⁴⁴ (G). Cys157 is located internally to the two vertebrate Mylpf structures (F, G). Color coding in (D)–(G) is the same as in (A).

(H) Alignment of human regulatory and essential light chain proteins highlighting conservation of Ala33, Gly163, and Cys157. The tissue that express each ortholog is indicated as follows: embryonic skeletal muscle (Emb), fast-twitch skeletal muscle (Fast), slow-twitch skeletal muscle (Slow), cardiac muscle (Card), and non-sarcomeric tissue (NS). The first residue in the shown aligned portions are numbered for each protein. Proteins in (H) are arranged by their similarity to MYLPPF.

C

Species	Gene	AA	"Ala33"	AA	"Cys157"	"Gly163"	%ident.
Human	MYLPPF	33	K E A F T V	152	D Y K N I C Y V I I T	- H G D A K K D	n/a
Rabbit	Mylpf	34	K E A F T V	153	D Y K N I C Y V I I T	- H G D A K K D	96.5
Mouse	Mylpf	33	K E A F T V	152	D Y K N I C Y V I I T	- H G D A K K D	95.9
Chicken	Mylpf	32	K E A F T V	151	D Y K N I C Y V I I T	- H G E D K K E	87.0
X. Trop	Mylpf	34	K E A F T V	153	D Y K N I C Y V I I T	- H G E D K D K	87.1
Danio	Mylpfa	34	K E A F T I	153	D Y K N I C Y V I I T	- H G E E K K E	80.5
Danio	Mylpfb	34	K E A F T I	153	D Y K N I C Y V I I T	- H G E E K K E	81.2
Shark	Mlc2	33	K E A F T V	152	D Y K N I C Y V I I T	- H G E E K D K	85.8
Hagfish	Mlc2	28	K E A F T I	147	D Y K N L C Y V I I T	- H G E E K K E	62.5
Squid	Mlc2	21	K E A F T M	138	N Y N K M V D - I I -	- K G K A E D	43.2
Fruit fly	Mlc2	83	K E A F Q L	140	D T A A L I E M L T G K	G G E E E E E	29.4
Scallop	Mlc2	23	K E A F S M	202	D Y V K F T A M I I -	- K G S G E E E	35.2
Dicty	Mlc2	28	K E A F E L	149	K Y D L F V N T L F -	- S K K	31.1
Yeast	Mlc2	23	K D A F Q M	148	E E R T F R G K L F -	- L D S I T D	17.6

D Scallop **E** Squid **F** Chicken **G** Rabbit

H

	Human Gene	AA	"Ala33"	AA	"Cys157"	"Gly163"	Expression
Regulatory	MYLPPF	33	A F T V	152	D Y K N I C Y V I I T H G D A		Fast + Emb
	MLC2	32	A F T I	151	D Y K N L V H I I T H G E E		Card + Slow
	MLC10	92	A F T I	211	D Y R N L C Y V I I T H G E E		NS
	MLC5	38	A F T L	157	D Y K A L S Y V I I T H G E E		Emb + NS
	MLC7	40	A F S C	159	D Y K S L C Y I I I T H G D E		Card
	MLC12B	37	A F N M	155	N Y I E F T R I L K H G A K		NS
	MLC12A	36	A F N M	154	N Y I E F T R I L K H G A K		NS
Essential	MLC6_1	15	A F Q L	140	N Y E A F V R H I L S G		NS
	MLC6_2	15	A F Q L	140	N Y E E L V R M V L N G		NS
	MLC4	59	A F S L	186	N Y E A F V K H I M S G		Card + Slow
	MLC3	57	A F M L	184	N Y E A F V K H I M S S		Fast
	MLC1	58	A F L L	183	N Y E A F V K H I M S I		Fast + Slow

protein model of the rabbit Mylpf-Myl1-Myosin heavy chain-Actin complex (PDB: 5H53)⁴⁴ (Figures 5A and 5B). Rabbit Mylpf protein is shifted one amino acid relative to the corresponding residues in the human counterparts (Figure 5C), but for simplicity, we refer to equivalent MYLPPF/Mylpf residues using human numbering across species. Ala33 is conserved in all eukaryotes examined, Gly163 is deeply conserved from scallop to human, but Cys157 is conserved only among vertebrates (Figure 5C). The protein model reveals that Ala33 is positioned adjacent to the myosin heavy chain and Mylpf Gly163 directly contacts a phenylalanine near the hook region of myosin heavy chain (Figure 5A). In contrast, Mylpf Cys157 is buried deep within the regulatory light chain and makes no contact with myosin heavy chain (Figure 5A).

To determine whether the interaction between Mylpf Gly163 and myosin heavy chain is conserved, we compared crystal structures of scallop, squid, and chicken myosin light and heavy chains to the rabbit structure (Figures 5D–5G; structures generated in Li et al.,³⁹ Himmel et al.,⁴¹ Yang et al.,⁴² and Wu et al.⁴³). In chicken, as in rabbit, Gly163 directly contacts a phenylalanine residue in the heavy chain (Figures 5F and 5G). Gly163 is found on the surface of the RLC in scallop and positioned very close the myosin heavy chain in squid (Figures 5D and 5E). Because Gly163 is present in animals that diverged from vertebrates prior to regulatory light chain gene family diversification, we reasoned that MYLPPF orthologs may also contain this residue. Alignment of human MYLPPF orthologs reveals perfect conservation of glycine in the

position corresponding to human Gly163. Some essential light chain proteins also have a corresponding glycine, suggesting that it arose very early in light chain gene evolution (Figure 5H). Likewise, Ala33 is conserved in all light chains examined including both ELCs and RLCs and is positioned close to the heavy chain in the crystal structures examined (Figures 5C–5H). In contrast, only three of the eight human regulatory light chain genes contain a cysteine in the Cys157 position (Figure 5H), revealing that although Cys157 is conserved among vertebrate Mylpf genes (Figure 5C), some orthologous regulatory light chain genes have a different residue in this position. Together these findings indicate that Ala33 arose prior to animal evolution, Gly163 arose early in animal evolution, and these residues directly or almost directly contact the myosin heavy chain in vertebrates. These observations suggest that the *MYLPF* p.Ala33Val and p.Gly163Ser variants have dominant effects because they more directly impact interactions with myosin heavy chain than the Cys157 variants.

Discussion

We identified four pathogenic variants in *MYLPF* in 8 unrelated families in which 17 affected individuals share similar phenotypic features, suggesting that mutations in *MYLPF* underlie a previously unrecognized multiple malformation syndrome. This condition is characterized by multiple congenital contractures, scoliosis, and short stature and is clinically indistinguishable from DA1 due to mutations in genes encoding other components of the contractile apparatus (e.g., embryonic myosin, troponins, tropomyosin). However, we find that short stature and proximal joint contractures (i.e., elbows, hips, knees) appear more commonly in DA1 due to variants in *MYLPF* than in DA1 due to other variants in other genes (*MYH3*, *TNNI2*, *TNNT3*, and *TPM2*).^{5,6} Nevertheless, because the number of families with pathogenic variants reported is small, the extent of overlap between their phenotypic features and those of individuals with variants in *MYH3*, *TNNI2*, *TPM2*, and *TNNT3* remains to be determined.

In contrast to the clinical findings of DA1 specifically, and of DAs in general, a single individual had segmental amyoplasia of the foot with fatty replacement of the muscle. We did not observe this finding in other persons with DA due to *MYLPF* variants, but we lacked pathological or imaging data of the limbs for all but one additional case, an affected fetus that underwent post-mortem exam at 19 weeks. Whether this is a finding in other individuals with pathogenic variants in *MYLPF* is unclear. To our knowledge, complete absence of limb skeletal muscles in a person with DA has not been reported. Hypoplasia or aplasia of the muscles of the upper and/or lower limbs is the defining feature of a group of arthrogryposis conditions known as amyoplasia.

Amyoplasia is the most common condition referred to as arthrogryposis, accounting for ~30% of all persons diagnosed with arthrogryposis.⁵⁰ The etiology is suspected to be heterogeneous (i.e., vascular disruption, monogenic, somatic mosaicism, oligogenic, etc.) and the heritability of amyoplasia, if any, remains unknown. The overwhelming majority of cases of amyoplasia are simplex, but rare instances of affected siblings have been reported. In such cases, amyoplasia is typically limited to either the upper or lower limbs.⁵¹ In a small subset of such families with lower limb amyoplasia (LLA), pathogenic variants have been found in one of several genes including *BICD2*,⁵² *CACNA1H*,⁵³ *DYNC1H1*,⁵⁴ *TRPV4*,⁵⁵ and *FKBP10*.⁵⁶ In each of the LLA conditions resulting from pathogenic variants in these genes, neurological abnormalities including weakness and hypotonia are typically present, distinguishing them from DA1 due to *MYLPF* variants. However, absence or severe atrophy of select muscles of the lower limbs is also common, if not typical, in these conditions, suggesting segmental amyoplasia is a genetically heterogeneous trait. Moreover, these observations suggest that, at least in some families with amyoplasia, large effect risk allele(s) might be segregating.

Our findings indicate that DA1 due to pathogenic variants in *MYLPF* can be transmitted as either an autosomal-dominant or autosomal-recessive condition. Nearly 400 genes underlying Mendelian conditions transmitted in both dominant and recessive inheritance patterns have been reported (J.X. Chong et al., 2019, Am. Soc. Hum. Genet., abstract). In the majority of these instances, the resulting Mendelian conditions have overlapping but different phenotypic features suggesting that while the inheritance patterns may differ, the pathogenesis for each is similar. In some cases, including DA1 due to variants in *MYLPF*, the clinical characteristics of the dominant and recessive conditions are virtually indistinguishable (e.g., cataracts due to variants in *CRYAA*). Differences in inheritance patterns can result from a variety of phenomena, including variants that affect distinct functional domains, result in loss versus gain of function, affect different tissue-specific transcripts, and have dose-dependent effects on gene function.

Substitutions of Gly163 and Ala33 in *MYLPF* both result in dominant DA1 whereas substitution of Cys157 underlies recessive DA1. These three residues are each conserved among all vertebrate *MYLPF* homologs, but Ala33 and Gly163 are more deeply conserved than Cys157. Indeed, Ala33 is found in all light chain genes examined and Gly163 is found in all animal RLC genes reviewed. This broad conservation suggests that Ala33 and Gly163 are vital to RLC identity. These two residues sit on the surface of *MYLPF* that contacts MyHC, whereas Cys157 is buried within *MYLPF*. This indicates that Ala33 and Gly163 might directly participate in critical protein-protein interactions and that the Ala33 and Gly163 mutants may reduce the binding affinity of *MYLPF* to the myosin lever arm; alternatively, the mutant *MYLPF* binding affinity may be normal

but results in an altered myosin structure. Such perturbation may directly affect the packing of MyHC molecules into the thick filament, which might in turn alter the function of other nearby myosins in this multimeric structure. In comparison, disruption of MYLPF amino acid residues that are positioned further from MyHC (e.g., Cys157) may result in lesser adverse effects on force transduction.

Based on the rabbit crystal structure, Ala33 and Gly163 may contact residues in human embryonic myosin, MYH3, that are affected in other DA conditions. Specifically, Gly163 is predicted to directly contact a phenylalanine residue in the MyHC that corresponds to Phe835 in MYH3. We previously reported an alteration at this MYH3 residue (c.2503_2505delTTC; p.Phe835del) in an individual with DA2A, the most severe of DA conditions. Similarly, Ala33 is positioned directly adjacent to a residue in MyHC that corresponds to MYH3 Lys838, a residue that we previously reported to be altered (c.2512A>G; p.Lys838Glu) in an individual with DA2B. In both cases, the condition (DA1) resulting from perturbation of MYLPF is less severe than the conditions (DA2A and DA2B) due to altering corresponding residues in MYH3. This difference in disease severity may reflect differences in protein function as MYLPF is thought to act primarily by stabilizing MyHC structure.^{7,57} We predict that other deeply conserved MYLPF residues that are positioned adjacent to disease-associated MyHC residues, such as MYLPF residues Glu29 and Glu32, may, if altered, also lead to dominantly inherited DA1.

We showed that myosin extracted from *mylpfa*-deficient zebrafish moves actin filaments more slowly than wild-type myosin extracts. The slowing (~75% of full speed) is less pronounced than was found in previous studies which removed myosin RLCs *in vitro* (~33% of full speed)^{8,9} and compared to *in vitro* extracted chicken myosin bearing a point mutation in Mylpf p.Phe102Leu (~50% of full speed).⁵⁸ We speculate that the effect of *mylpfa* loss is milder than was seen in these previous assays because the mutant still has some RLC function, provided by *mylpfb* in fast fibers and by a normal set of RLCs in slow-twitch fibers. Our findings suggest that *mylpfb* cannot fully compensate for *mylpfa* loss, because the *mylpfa* single mutant shows modest loss of actin motility, a dramatic reduction of total trunk muscle force, and complete pectoral fin paralysis. However, the degree of the compensation, if any, remains to be assessed. Nevertheless, loss of *mylpfa* alone parallels the phenotypic consequences observed in DA1, and DAs in general, in which the more distal body areas (e.g., hands versus shoulders) are more frequently and more severely affected.

In addition to muscle weakness and pectoral fin paralysis, zebrafish *mylpfa* mutant muscle fibers eventually degenerate in all muscles, with the PHM being most severely affected. This degeneration indicates that Mylpf function is essential for muscle integrity during early development and suggests mechanisms for muscle loss in humans with DA1. *Mylpfa* is a marker of fast-twitch myofibers and is abundantly expressed in PHM whereas there

are few *smyhc2*-positive slow twitch fibers and no *smyhc1*-positive slow-twitch fibers in the PHM, suggesting that it is composed largely of fast-twitch myofibers.^{23,30,49} In contrast, slow-twitch myofibers are more common in myotomes where they may exert a stabilizing effect. Our finding that the PHM is most strongly affected is consistent with the observation that the most severe contractures in DA1, as well as muscle hypoplasia and/or aplasia, occur more frequently in the most distal regions of the limb (e.g., digits, hands, wrists, feet, and ankles). Muscle fibers in myotomes also become irregularly shaped over time in *mylpfa* knockouts, consistent with the observation that the trunk muscles of persons with DA1 due to *MYLPF* variants are typically affected but more mildly than the limbs.

In summary, we discovered that variants in *MYLPF* underlie both dominant and recessive forms of a distal arthrogyposis with features typically seen in DA1. The distribution of these features in persons with DA1 due to *MYLPF* variants largely overlaps that of DA1 due to variants in *MYH3*, *TNNI2*, *TPM2*, and *TNNT3*, with proximal joint contractures perhaps more common in individuals with *MYLPF* variants. However, segmental amyoplasia appears to be a unique feature of DA1 due to *MYLPF* that, based on knockout of *mylpfa* in zebrafish, results from degeneration of differentiated skeletal myofibers.

Data and Code Availability

Sequence data for families A and B are pending submission to dbGaP but no accession numbers are available yet. Please contact the corresponding author M.J.B. for further information. *MYLPF* variants were deposited in ClinVar VCV000916685, VCV000916686, VCV000916687, and VCV000916688.

Supplemental Data

Supplemental Data can be found online at <https://doi.org/10.1016/j.ajhg.2020.06.014>.

Acknowledgments

We thank the families for their participation and support. Sequencing for families A and B was provided by the University of Washington Center for Mendelian Genomics (UW-CMG) and was funded by NHGRI and NHLBI grants UM1 HG006493 and U24 HG008956, by the Office of the Director, NIH under Award Number S10OD021553, and by the National Institute of Child Health and Human Development (1R01HD048895 to M.J.B.). We thank the Ohio State Rightmire Hall zebrafish staff for excellent animal care and husbandry and Mark Nilan and Mika Gallati for zebrafish care and mutant identification at the University of Maine. We thank Sarah Shepherd for assistance during initial *mylpfa*^{oz43} construction. Zebrafish work was funded by NIH grants GM088041 and GM117964 (to S.L.A.), an NIH T32 training grant NS077984 and an Ohio State Pelotonia postdoctoral fellowship (to J.C.T.), Ohio State Edward Mayers and Elizabeth Wagner research scholarships (to E.M.T.), and NIH HL150953 and AR067279 (to D.M.W.). The

Ohio State Neuroscience Imaging Core facilities are supported by NIH grants P30-NS045758, P30-NS104177, and S10-OD010383. We acknowledge the DNA Sequencing Shared Resource at The Ohio State University Comprehensive Cancer Center. This work was also supported by the Indian Council of Medical Research, Government of India (No.5/13/58/2015/NCD-III). The F310 antibody developed by Frank Stockdale was obtained from the Developmental Studies Hybridoma Bank, created by the NICHD of the NIH and maintained at The University of Iowa, Department of Biology. The authors are grateful to Mrs. Séverine Drouhin and to the Molecular Biology Facility of the Grenoble University Hospital, France for technical assistance. The content is solely the responsibility of the authors and does not necessarily represent the official views of the National Institutes of Health.

Declaration of Interests

The authors declare no competing interests.

Received: May 2, 2020

Accepted: June 18, 2020

Published: July 23, 2020

Web Resources

ClinVar, <https://www.ncbi.nlm.nih.gov/clinvar/>
EMBL-EBI expression atlas, <https://www.ebi.ac.uk/gxa/home>
GenBank, <https://www.ncbi.nlm.nih.gov/genbank/>
Geno2MP, <https://geno2mp.gs.washington.edu/Geno2MP/>
gnomAD, <https://gnomad.broadinstitute.org>
Human Genome Variation, <http://www.hgvs.org/mutnomen/>
OMIM, <https://www.omim.org/>
PDB, <http://www.rcsb.org/>
UniProt, <http://www.uniprot.org/>

References

- Bamshad, M., Jorde, L.B., and Carey, J.C. (1996). A revised and extended classification of the distal arthrogyposes. *Am. J. Med. Genet.* *65*, 277–281.
- Bamshad, M., Bohnsack, J.F., Jorde, L.B., and Carey, J.C. (1996). Distal arthrogyposis type 1: clinical analysis of a large kindred. *Am. J. Med. Genet.* *65*, 282–285.
- Stevenson, D.A., Carey, J.C., Palumbos, J., Rutherford, A., Dolcourt, J., and Bamshad, M.J. (2006). Clinical characteristics and natural history of Freeman-Sheldon syndrome. *Pediatrics* *117*, 754–762.
- Krakowiak, P.A., Bohnsack, J.F., Carey, J.C., and Bamshad, M. (1998). Clinical analysis of a variant of Freeman-Sheldon syndrome (DA2B). *Am. J. Med. Genet.* *76*, 93–98.
- Beck, A.E., McMillin, M.J., Gildersleeve, H.I.S., Shively, K.M.B., Tang, A., and Bamshad, M.J. (2014). Genotype-phenotype relationships in Freeman-Sheldon syndrome. *Am. J. Med. Genet. A* *164A*, 2808–2813.
- Toydemir, R.M., Rutherford, A., Whitby, F.G., Jorde, L.B., Carey, J.C., and Bamshad, M.J. (2006). Mutations in embryonic myosin heavy chain (MYH3) cause Freeman-Sheldon syndrome and Sheldon-Hall syndrome. *Nat. Genet.* *38*, 561–565.
- Lowey, S., and Trybus, K.M. (2010). Common structural motifs for the regulation of divergent class II myosins. *J. Biol. Chem.* *285*, 16403–16407.
- Lowey, S., Waller, G.S., and Trybus, K.M. (1993). Skeletal muscle myosin light chains are essential for physiological speeds of shortening. *Nature* *365*, 454–456.
- VanBuren, P., Waller, G.S., Harris, D.E., Trybus, K.M., Warshaw, D.M., and Lowey, S. (1994). The essential light chain is required for full force production by skeletal muscle myosin. *Proc. Natl. Acad. Sci. USA* *91*, 12403–12407.
- Wang, Y., Szczesna-Cordary, D., Craig, R., Diaz-Perez, Z., Guzman, G., Miller, T., and Potter, J.D. (2007). Fast skeletal muscle regulatory light chain is required for fast and slow skeletal muscle development. *FASEB J.* *21*, 2205–2214.
- Goody, M.F., Carter, E.V., Kilroy, E.A., Maves, L., and Henry, C.A. (2017). “Muscling” Throughout Life: Integrating Studies of Muscle Development, Homeostasis, and Disease in Zebrafish. *Curr. Top. Dev. Biol.* *124*, 197–234.
- Jackson, H.E., and Ingham, P.W. (2013). Control of muscle fibre-type diversity during embryonic development: the zebrafish paradigm. *Mech. Dev.* *130*, 447–457.
- Li, M., Hromowyk, K.J., Amacher, S.L., and Currie, P.D. (2017). Muscular dystrophy modeling in zebrafish. *Methods Cell Biol.* *138*, 347–380.
- Talbot, J., and Maves, L. (2016). Skeletal muscle fiber type: using insights from muscle developmental biology to dissect targets for susceptibility and resistance to muscle disease. *Wiley Interdiscip. Rev. Dev. Biol.* *5*, 518–534.
- Bird, N.C., Windner, S.E., and Devoto, S.H. (2011). Immunocytochemistry to study myogenesis in zebrafish. *Methods Mol. Biol.* *798*, 153–169.
- Devoto, S.H., Melançon, E., Eisen, J.S., and Westerfield, M. (1996). Identification of separate slow and fast muscle precursor cells in vivo, prior to somite formation. *Development* *122*, 3371–3380.
- Kimmel, C.B., Ballard, W.W., Kimmel, S.R., Ullmann, B., and Schilling, T.F. (1995). Stages of embryonic development of the zebrafish. *Dev. Dyn.* *203*, 253–310.
- Xu, Y., He, J., Wang, X., Lim, T.M., and Gong, Z. (2000). Asynchronous activation of 10 muscle-specific protein (MSP) genes during zebrafish somitogenesis. *Dev. Dyn.* *219*, 201–215.
- Haines, L., Neyt, C., Gautier, P., Keenan, D.G., Bryson-Richardson, R.J., Hollway, G.E., Cole, N.J., and Currie, P.D. (2004). Met and Hgf signaling controls hypaxial muscle and lateral line development in the zebrafish. *Development* *131*, 4857–4869.
- Masselink, W., Cole, N.J., Fenyés, F., Berger, S., Sonntag, C., Wood, A., Nguyen, P.D., Cohen, N., Knopf, F., Weidinger, G., et al. (2016). A somitic contribution to the apical ectodermal ridge is essential for fin formation. *Nature* *535*, 542–546.
- Minchin, J.E.N., Williams, V.C., Hinits, Y., Low, S., Tandon, P., Fan, C.-M., Rawls, J.F., and Hughes, S.M. (2013). Oesophageal and sternohyal muscle fibres are novel Pax3-dependent migratory somite derivatives essential for ingestion. *Development* *140*, 2972–2984.
- Neyt, C., Jagla, K., Thisse, C., Thisse, B., Haines, L., and Currie, P.D. (2000). Evolutionary origins of vertebrate appendicular muscle. *Nature* *408*, 82–86.
- Talbot, J.C., Teets, E.M., Ratnayake, D., Duy, P.Q., Currie, P.D., and Amacher, S.L. (2019). Muscle precursor cell movements in zebrafish are dynamic and require Six family genes. *Development* *146*, dev171421.
- Chong, J.X., Buckingham, K.J., Jhangiani, S.N., Boehm, C., Sobreira, N., Smith, J.D., Harrell, T.M., McMillin, M.J., Wiszniewski, W., Gambin, T., et al.; Centers for Mendelian Genomics

- (2015). The Genetic Basis of Mendelian Phenotypes: Discoveries, Challenges, and Opportunities. *Am. J. Hum. Genet.* *97*, 199–215.
25. McLaren, W., Gil, L., Hunt, S.E., Riat, H.S., Ritchie, G.R.S., Thormann, A., Flicek, P., and Cunningham, F. (2016). The Ensembl Variant Effect Predictor. *Genome Biol.* *17*, 122.
 26. Paila, U., Chapman, B.A., Kirchner, R., and Quinlan, A.R. (2013). GEMINI: integrative exploration of genetic variation and genome annotations. *PLoS Comput. Biol.* *9*, e1003153.
 27. Westerfield, M. (2007). *The Zebrafish Book: A guide for the laboratory use of zebrafish (Danio rerio)* (University of Oregon Press).
 28. Ignatius, M.S., Chen, E., Elpek, N.M., Fuller, A.Z., Tenente, I.M., Clagg, R., Liu, S., Blackburn, J.S., Linardic, C.M., Rosenberg, A.E., et al. (2012). In vivo imaging of tumor-propagating cells, regional tumor heterogeneity, and dynamic cell movements in embryonal rhabdomyosarcoma. *Cancer Cell* *21*, 680–693.
 29. Tang, Q., Moore, J.C., Ignatius, M.S., Tenente, I.M., Hayes, M.N., Garcia, E.G., Torres Yordán, N., Bourque, C., He, S., Blackburn, J.S., et al. (2016). Imaging tumour cell heterogeneity following cell transplantation into optically clear immune-deficient zebrafish. *Nat. Commun.* *7*, 10358.
 30. Elworthy, S., Hargrave, M., Knight, R., Mebus, K., and Ingham, P.W. (2008). Expression of multiple slow myosin heavy chain genes reveals a diversity of zebrafish slow twitch muscle fibres with differing requirements for Hedgehog and Prdm1 activity. *Development* *135*, 2115–2126.
 31. Hromowyk, K.J., Talbot, J.C., Martin, B.L., Janssen, P.M.L., and Amacher, S.L. (2020). Cell fusion is differentially regulated in zebrafish post-embryonic slow and fast muscle. *Dev. Biol.* *462*, 85–100.
 32. Talbot, J.C., and Amacher, S.L. (2014). A streamlined CRISPR pipeline to reliably generate zebrafish frameshifting alleles. *Zebrafish* *11*, 583–585.
 33. Berberoglu, M.A., Gallagher, T.L., Morrow, Z.T., Talbot, J.C., Hromowyk, K.J., Tenente, I.M., Langenau, D.M., and Amacher, S.L. (2017). Satellite-like cells contribute to pax7-dependent skeletal muscle repair in adult zebrafish. *Dev. Biol.* *424*, 162–180.
 34. Jowett, T. (1999). Analysis of protein and gene expression. *Methods Cell Biol.* *59*, 63–85.
 35. Martin, B.L., Gallagher, T.L., Rastogi, N., Davis, J.P., Beattie, C.E., Amacher, S.L., and Janssen, P.M.L. (2015). In vivo assessment of contractile strength distinguishes differential gene function in skeletal muscle of zebrafish larvae. *J. Appl. Physiol.* *119*, 799–806.
 36. Smith, L.L., Beggs, A.H., and Gupta, V.A. (2013). Analysis of skeletal muscle defects in larval zebrafish by birefringence and touch-evoke escape response assays. *J. Vis. Exp.* *9*, e50925.
 37. Warshaw, D.M., Desrosiers, J.M., Work, S.S., and Trybus, K.M. (1990). Smooth muscle myosin cross-bridge interactions modulate actin filament sliding velocity in vitro. *J. Cell Biol.* *111*, 453–463.
 38. Palmiter, K.A., Tyska, M.J., Haeberle, J.R., Alpert, N.R., Fananapazir, L., and Warshaw, D.M. (2000). R403Q and L908V mutant β -cardiac myosin from patients with familial hypertrophic cardiomyopathy exhibit enhanced mechanical performance at the single molecule level. *J. Muscle Res. Cell Motil.* *21*, 609–620.
 39. Li, A., Nelson, S.R., Rahmanseresht, S., Braet, F., Cornachione, A.S., Previs, S.B., O'Leary, T.S., McNamara, J.W., Rassier, D.E., Sadayappan, S., et al. (2019). Skeletal MyBP-C isoforms tune the molecular contractility of divergent skeletal muscle systems. *Proc. Natl. Acad. Sci. USA* *116*, 21882–21892.
 40. Papatheodorou, I., Fonseca, N.A., Keays, M., Tang, Y.A., Barera, E., Bazant, W., Burke, M., Füllgrabe, A., Fuentes, A.M.-P., George, N., et al. (2018). Expression Atlas: gene and protein expression across multiple studies and organisms. *Nucleic Acids Res.* *46* (D1), D246–D251.
 41. Himmel, D.M., Gourinath, S., Reshetnikova, L., Shen, Y., Szent-Györgyi, A.G., and Cohen, C. (2002). Crystallographic findings on the internally uncoupled and near-rigor states of myosin: further insights into the mechanics of the motor. *Proc. Natl. Acad. Sci. USA* *99*, 12645–12650.
 42. Yang, Y., Gourinath, S., Kovács, M., Nyitray, L., Reutzel, R., Himmel, D.M., O'Neill-Hennessey, E., Reshetnikova, L., Szent-Györgyi, A.G., Brown, J.H., and Cohen, C. (2007). Rigor-like structures from muscle myosins reveal key mechanical elements in the transduction pathways of this allosteric motor. *Structure* *15*, 553–564.
 43. Wu, S., Liu, J., Reedy, M.C., Tregear, R.T., Winkler, H., Franzini-Armstrong, C., Sasaki, H., Lucaveche, C., Goldman, Y.E., Reedy, M.K., and Taylor, K.A. (2010). Electron tomography of cryofixed, isometrically contracting insect flight muscle reveals novel actin-myosin interactions. *PLoS ONE* *5*, e12643.
 44. Fujii, T., and Namba, K. (2017). Structure of actomyosin rigour complex at 5.2Å resolution and insights into the ATPase cycle mechanism. *Nat. Commun.* *8*, 13969.
 45. Heissler, S.M., and Sellers, J.R. (2014). Myosin light chains: Teaching old dogs new tricks. *Bioarchitecture* *4*, 169–188.
 46. Reiser, P.J. (2019). Current understanding of conventional and novel co-expression patterns of mammalian sarcomeric myosin heavy chains and light chains. *Arch. Biochem. Biophys.* *662*, 129–133.
 47. Sitbon, Y.H., Yadav, S., Kazmierczak, K., and Szczesna-Cordary, D. (2019). Insights into myosin regulatory and essential light chains: a focus on their roles in cardiac and skeletal muscle function, development and disease. *J. Muscle Res. Cell Motil.* *9*, 1–15.
 48. Wagner, D.E., Weinreb, C., Collins, Z.M., Briggs, J.A., Megason, S.G., and Klein, A.M. (2018). Single-cell mapping of gene expression landscapes and lineage in the zebrafish embryo. *Science* *360*, 981–987.
 49. Patterson, S.E., Mook, L.B., and Devoto, S.H. (2008). Growth in the larval zebrafish pectoral fin and trunk musculature. *Dev. Dyn.* *237*, 307–315.
 50. Hall, J.G., Aldinger, K.A., and Tanaka, K.I. (2014). Amyoplasia revisited. *Am. J. Med. Genet. A.* *164A*, 700–730.
 51. Hall, J.G. (2014). Amyoplasia involving only the upper limbs or only involving the lower limbs with review of the relevant differential diagnoses. *Am. J. Med. Genet. A.* *164A*, 859–873.
 52. Frasquet, M., Camacho, A., Vílchez, R., Argente-Escrig, H., Millet, E., Vázquez-Costa, J.F., Silla, R., Sánchez-Monteaigudo, A., Vílchez, J.J., Espinós, C., et al. (2020). Clinical spectrum of BICD2 mutations. *Eur. J. Neurol.* *27*, 1327–1335.
 53. Carter, M.T., McMillan, H.J., Tomin, A., and Weiss, N. (2019). Compound heterozygous CACNA1H mutations associated with severe congenital amyotrophy. *Channels (Austin)* *13*, 153–161.
 54. Scoto, M., Rossor, A.M., Harms, M.B., Cirak, S., Calissano, M., Robb, S., Manzur, A.Y., Martínez Arroyo, A., Rodríguez Sanz, A., Mansour, S., et al. (2015). Novel mutations expand the clinical spectrum of DYNC1H1-associated spinal muscular atrophy. *Neurology* *84*, 668–679.
 55. Velilla, J., Marchetti, M.M., Toth-Petroczy, A., Grosogeat, C., Bennett, A.H., Carmichael, N., Estrella, E., Darras, B.T., Frank, N.Y., Krier, J., et al. (2019). Homozygous *TRPV4* mutation

- causes congenital distal spinal muscular atrophy and arthrogryposis. *Neurol. Genet.* 5, e312.
56. Barnes, A.M., Duncan, G., Weis, M., Paton, W., Cabral, W.A., Mertz, E.L., Makareeva, E., Gambello, M.J., Lachawan, F.L., Leikin, S., et al. (2013). Kuskokwim syndrome, a recessive congenital contracture disorder, extends the phenotype of FKBP10 mutations. *Hum. Mutat.* 34, 1279–1288.
57. Pastra-Landis, S.C., and Lowey, S. (1986). Myosin subunit interactions. Properties of the 19,000-dalton light chain-deficient myosin. *J. Biol. Chem.* 261, 14811–14816.
58. Sherwood, J.J., Waller, G.S., Warshaw, D.M., and Lowey, S. (2004). A point mutation in the regulatory light chain reduces the step size of skeletal muscle myosin. *Proc. Natl. Acad. Sci. USA* 101, 10973–10978.